Chemical Engineering Journal 507 (2025) 160485

Contents lists available at ScienceDirect

Chemical Engineering Journal

journal homepage: www.elsevier.com/locate/cej

Antimicrobial resistance control by liquid ground-electrode dielectric barrier discharge Plasma: The importance of oxidative reactive species

Ruoyu Deng [a,b], Qiang He [a], Liang Luo [a,b], Dongxu Yang [a], Yi Sun [a], Yi Chen [a,*]

[a] Key Laboratory of the Three Gorges Reservoir Region's Eco-Environment, Ministry of Education, Chongqing University, Chongqing 400045 China
[b] CAS Key Laboratory of Urban Pollutant Conversion, Department of Environmental Science and Technology, University of Science and Technology of China, Hefei 230026 China

ARTICLE INFO

Keywords:
Antibiotic resistant bacteria
Antibiotic resistance genes
Dielectric barrier discharge plasma
Oxidative reactive species
Basic discharge unit model

ABSTRACT

The widespread dissemination of antibiotic resistant bacteria (ARB) and antibiotic resistance genes (ARGs) poses a significant threat to global public health and environmental safety. Conventional disinfection methods always fail to prevent ARG transmission, sometimes even exacerbating antimicrobial resistance (AMR). In this study, we developed a liquid ground-electrode dielectric barrier discharge (lgDBD) plasma process to mitigate ARB (*Escherichia coli* MG1655 carrying the plasmid RP4) and ARGs (AmpR, TetA, and KanR) that demonstrated rapid and effective performance: under a 12 kV voltage, a 6.90-log reduction in ARB was achieved within 6 min, with an ARG removal efficiency exceeding 2.74-log copies/mL within 10 min. The electrical energy per order (E_{EO}) for ARB and ARGs removal was only 0.268 kWh·m^{-3} and 0.975–1.125 kWh·m^{-3}, respectively, significantly outperforming other disinfection processes that rely on electrical energy. Moreover, lgDBD significantly suppressed intragenus and intergenus conjugative transfer, with maximum reductions of 98.6 % and 98.1 %, respectively. A finite element model was also employed to analyze the spatiotemporal distribution of reactive species in the basic discharge unit, and this revealed that free oxygen atoms and O(^{1}D) play critical roles in the generation and reactions of oxidative reactive species (ORSs). The oxidation of essential biomolecules by ORSs effectively blocks the transmission of ARGs, and the electroporation induced by the strong electric field further facilitates this process. In summary, this study elucidates the mechanisms of ORSs generation and action in lgDBD and offers a promising solution for controlling antibiotic resistance pollution in aquatic environments.

1. Introduction

The growing prevalence of antibiotic resistant bacteria (ARB) and the spread of antibiotic resistance genes (ARGs) pose significant threats to global public health and environmental safety [1–3]. ARB and ARGs in aquatic environments are of particular concern, as horizontal gene transfer (HGT) facilitates the transmission of ARGs between different populations, increasing the risk of resistance dissemination [4,5]. Although traditional disinfection processes, such as chlorination and ultraviolet (UV) irradiation, have been widely employed for bacterial control [6–10], studies have shown that these methods often fail to completely inactivate ARB and have limited effectiveness in inhibiting the conjugative transfer of ARGs, sometimes even exacerbating bacterial resistance [11,12]. Therefore, innovative processes for efficiently controlling ARB and ARGs are urgently needed to address the challenges associated with the spread of antibiotic resistance in aquatic environments.

Advanced oxidation processes (AOPs) have been widely applied for bacterial inactivation and ARG removal [13–15]. Dielectric barrier discharge (DBD) is an emerging AOP that has recently garnered much attention with respect to its possible applications in water treatment, soil remediation, and air pollution control [16–20]. DBD plasma generates a variety of oxidative reactive species (ORSs), such as hydroxyl radicals (·OH), peroxynitrous acid (ONOOH), ozone (O_3), and hydrogen peroxide (H_2O_2), which can effectively inactivate bacteria and degrade contaminants [21–24]. Compared to conventional AOPs, DBD process offers advantages such as ambient temperature operation, no need for chemical reagents, and no secondary pollution [20,25,26]. However, the limited utilization of reactive species and low gas–liquid mass transfer efficiency have constrained the practical application of DBD in many applications where its potential benefits are the greatest [27–29].

To overcome the limitations of traditional DBD, a novel liquid

* Corresponding author.
E-mail address: chenyi8574@cqu.edu.cn (Y. Chen).

https://doi.org/10.1016/j.cej.2025.160485
Received 16 November 2024; Received in revised form 4 January 2025; Accepted 9 February 2025
Available online 10 February 2025
1385-8947/

ground-electrode dielectric barrier discharge (lgDBD) process has been developed [30]. The lgDBD process enhances the utilization and mass transfer efficiency of reactive species by allowing direct contact between the plasma and the target water [31]. It has demonstrated excellent performance in degrading organic micropollutants and disinfecting disinfection-residual-bacteria [32]. However, its potential to mitigate the risks associated with antibiotic resistance transmission requires further investigation. Additionally, understanding of the ORSs involved in the lgDBD process remains limited, primarily focused on reactions occurring in the liquid phase while neglecting those in the gas-phase plasma [33]. The generation of lgDBD plasma relies on applying high voltage across an insulating dielectric barrier which leads to the ionization of air and the production of free electrons [34]. These free electrons collide with air molecules to generate a variety of excited-state species. At the gas–liquid interface, these excited-state species undergo dissolution into the liquid phase or trigger interfacial reactions that form ORSs such as reactive oxygen species and reactive nitrogen species [35]. Although free electrons and their derived excited-state species play key roles in the formation and transformation of oxidative reactive species, their short lifetimes together with interference from complex multiphase systems make it difficult for conventional detection methods to elucidate these mechanisms completely.

In this study, *Escherichia coli* MG1655 that harbored an RP4 plasmid carrying three distinct types of ARGs (AmpR, TetA, and KanR) was used as a model ARB in order to evaluate the effects of lgDBD on ARB inactivation, ARG removal, and ARG conjugative transfer. Additionally, a finite element model of a basic discharge unit was employed to analyze the spatiotemporal distribution of reactive species during the lgDBD process. This study aims to elucidate the generation and action mechanisms of ORSs involved in the lgDBD process using the combined analysis of various reactive species and cell damage.

2. Materials and methods

2.1. Reagents and strains

Pure water and ultrapure water used in experiments were obtained from an ULUP-II-100 ultrapure water production system. All reagents and bacterial strains used in experiments are described in detail in Text S1.

2.2. Experimental setup

A detailed description of the experimental setup and the bacterial inactivation experiment is provided in Text S2. In the conjugation transfer experiments, *Escherichia coli* MG1655 (RP4) was inoculated in Luria-Bertani (LB) broth containing ampicillin (Amp) (200 mg/L) and tetracycline (Tet) (10 mg/L), *Escherichia coli* HB101 in LB was inoculated broth containing streptomycin (Str) (30 mg/L), and *Pseudomonas putida* GDMCC1.445 was inoculated in LB broth containing chloramphenicol (Chl) (30 mg/L), each followed by shaking incubation at 37 °C overnight for approximately 14 h. The cultures were then centrifuged at 3,000 rpm for 5 min and resuspended in phosphate-buffered saline (PBS). The bacterial suspensions were prepared in PBS to reach roughly 10^8 CFU/mL for use in conjugation transfer experiments. Next, one liter of the plasmid donor strain *Escherichia coli* MG1655 (RP4) was placed into the liquid-grounded electrode DBD reactor. After 10 min of lgDBD treatment at 9–12 kV, the bacterial suspension was centrifuged and resuspended in PBS. Five milliliters of the donor strain were mixed with 5 mL of *Escherichia coli* HB101 (for intraspecies conjugation) and 5 mL of *Pseudomonas putida* GDMCC1.445 (for interspecies conjugation) and incubated at 37 °C with shaking for 16 h. Receptor and transconjugant concentrations were determined using the plate-counting method. Intraspecies conjugation transconjugants were cultured on LB solid medium containing Amp (200 mg/L), Tet (10 mg/L), and Str (30 mg/L), and the receptor strain was cultured on LB solid medium containing Str (30 mg/L). Interspecies conjugation transconjugants were cultured on LB solid medium containing Amp (200 mg/L), Tet (10 mg/L), and Chl (30 mg/L), and the receptor strain was cultured on LB solid medium containing Chl (30 mg/L).

Detailed procedures for determining inactivation efficiency, discharge power, energy efficiency, and conjugative transfer frequency are provided in Text S3.

2.3. Analytical methods

For confocal microscopy analysis, the samples were stained with SYTO 9 and propidium iodide (PI) [36]. The absolute abundances of the ARGs (AmpR, TetA, and KanR) in the bacterial suspensions were measured using real-time PCR, and the antibiotic susceptibility of each strain was determined using the broth microdilution method [37–40]. A detailed description of the analytical methods can be found in Text S4.

Optical emission spectra (OES) were obtained using a high-resolution fiber optic spectrometer (ULS3648-USB2-UA-25). Electron paramagnetic resonance (EPR) spectra were acquired as spin traps on CIQTEK EPR200-Plus spectrometer with a scanning range of 3,300–3,400 G, a center field of 3,350 G, and a modulation frequency of 100 kHz in the signal channel. Reactive species quenching experiments employed TBA as the ·OH scavenger, BQ as the $O_2^{\cdot-}$ scavenger, and TEMP as the $^1O_2$ scavenger [30].

2.4. Simulation methods

Parallel streamer solver with kinetics (PASSKEy) code was used to construct a two-dimensional model of the basic discharge unit of the liquid-grounded electrode. A detailed description is provided in Text S5.

3. Results and Discussion

3.1. ARB inactivation by lgDBD process

Fig. 1a shows the log reduction rate of *Escherichia coli* MG1655 (RP4) in lgDBD under different input voltages. At an input voltage of 9 kV, *Escherichia coli* MG1655 (RP4) suffered a 6.58-log reduction within 10 min. As the input voltage increased, the inactivation rate exhibited a clear upward trend as well. At 12 kV, *Escherichia coli* MG1655 (RP4) suffered a 6.90-log reduction within 6 min and was completely inactivated (>7.00-log) within 8 min. This enhanced inactivation efficiency with increased input voltage can be attributed to the intensified degree of plasma ionization. The intensification promotes more frequent collisions between free electrons and gas molecules that leads to an increased generation of ORSs and thereby accelerates the inactivation process. Additionally, the strong electric field facilitates electroporation, resulting in increased cell membrane permeability and aiding the penetration of reactive species into bacterial cells [41,42]. Therefore, high input voltage effectively promotes bacterial inactivation, making lgDBD a promising technique for reducing ARB risk in water.

Fig. 1b further presents the variation trends in the pseudo-first-order kinetic rate constant and energy efficiency ($G_{6\text{-log}}$) for lgDBD inactivation of *Escherichia coli* MG1655 (RP4) under different input voltages. $G_{6\text{-log}}$ refers to the volume of water treated per unit energy consumption when achieving a 6-log reduction in bacteria. These results show that the kinetic rate constant increases with the input voltage, which aligns with the observed trend in the log reduction rate. The pseudo-first-order kinetic rate constant reached its maximum at 12 kV, at 1.135 CFU ml^{-1} min^{-1}. However, the energy efficiency $G_{6\text{-log}}$ exhibited a different pattern. It peaked at 11 kV (3,313.82 L/kWh), followed by 9 kV (3,124.95 L/kWh), and the energy efficiency at 12 kV (3,104.32 L/kWh) and 10 kV (2,571.6 L/kWh) was relatively lower. The optimal sterilization rate and energy efficiency were achieved at 12 kV and 11 kV, respectively. The discrepancy in these optimal voltages arises because higher input voltages enhance the sterilization rate by increasing

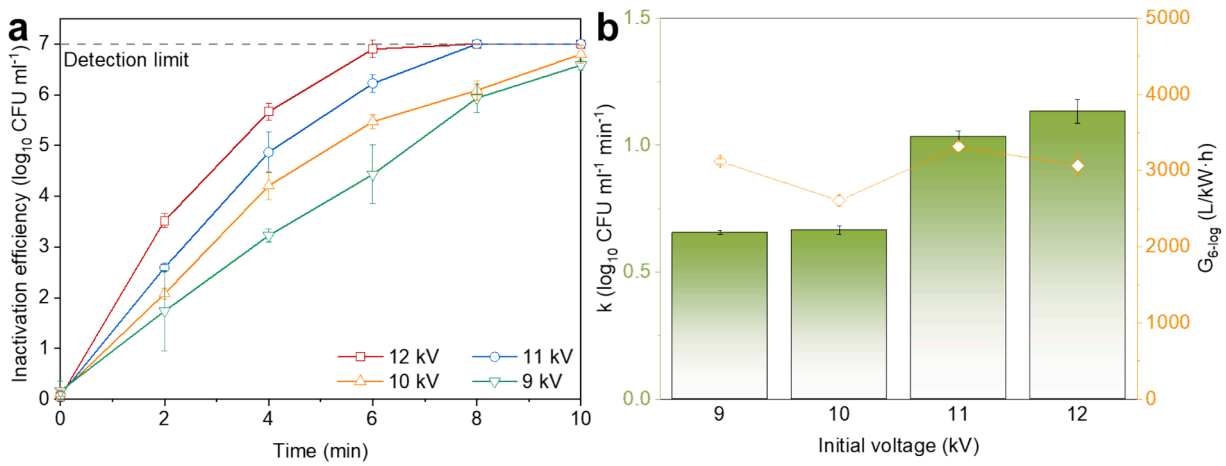

Fig. 1. (a) Logarithmic inactivation efficiency of *Escherichia coli* MG1655 (RP4) under various initial voltages; Conditions: bacterial initial concentration: 10^7 CFU/mL; pH: 7.0. (b)Pseudo-first-order inactivation rate constants and energy efficiencies at different initial voltages.

reactive species production, but they also significantly raise energy consumption [43–45]. Within the 9–11 kV range, increases in energy input yielded substantial efficiency gains, indicating that the energy was indeed effectively utilized. However, beyond 11 kV, further increases in energy input resulted in diminishing returns, as the additional energy consumption did not correspond to proportionate improvements in sterilization efficiency. This ultimately led to a decline in overall energy efficiency. Therefore, in practical applications it is crucial to select input voltage and other operational parameters carefully in order to meet required sterilization levels while balancing treatment efficiency and energy consumption for optimal performance.

3.2. ARG removal by lgDBD process

The absolute quantities of three ARGs, AmpR, TetA, and KanR, in the bacterial solution before and after lgDBD treatment were quantified using real-time PCR. To evaluate the removal effect of lgDBD on ARGs under different input voltages (9–12 kV), the concentrations of the three

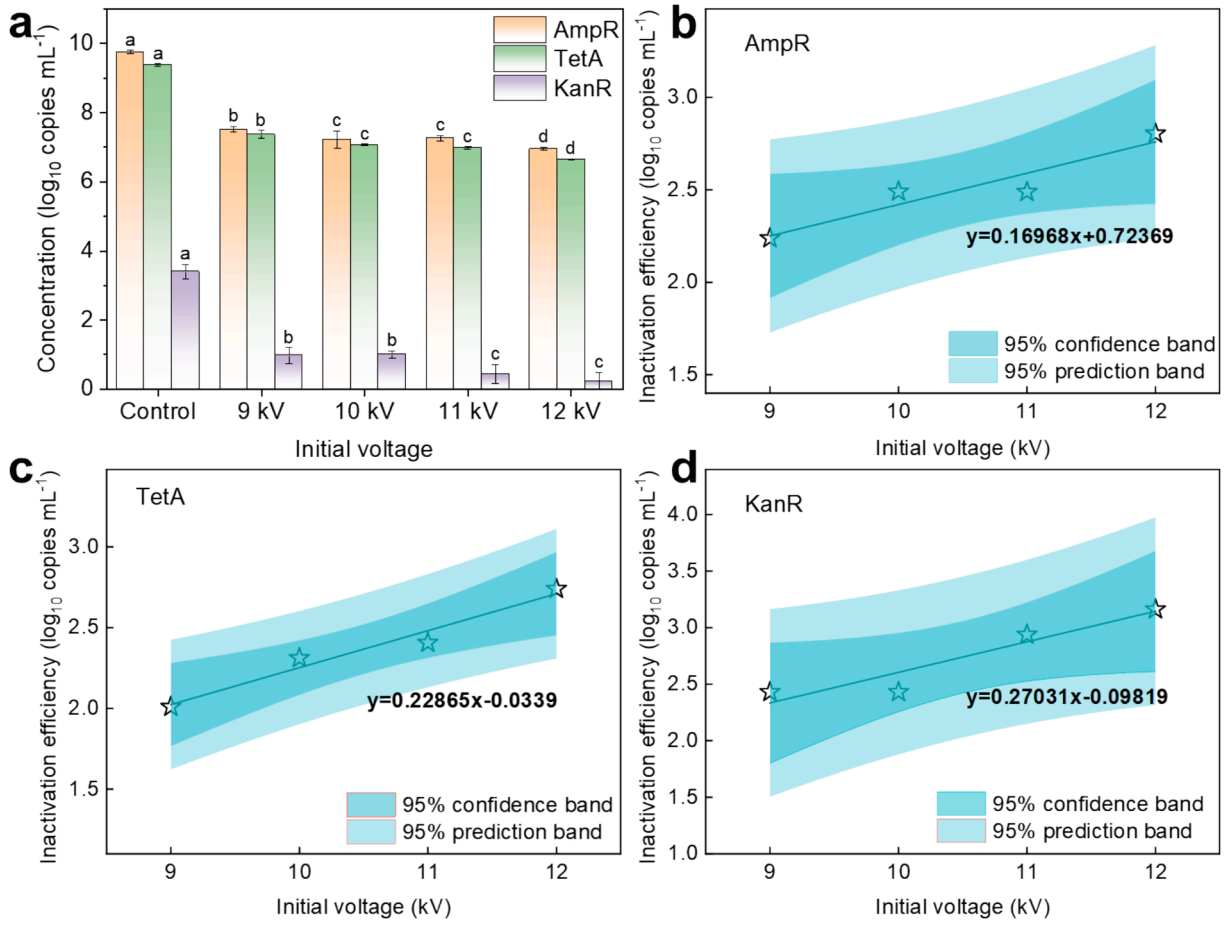

Fig. 2. The logarithmic degradation rates of AmpR, TetA and KanR in lgDBD at different voltages.

ARGs before and after treatment were compared. As shown in Fig. 2a, before lgDBD treatment, the initial concentrations of AmpR, TetA, and KanR were 5.810×10^9 copies/mL, 2.433×10^9 copies/mL, and 2,775 copies/mL, respectively. After 10 min of lgDBD treatment at 12 kV, however, all three ARGs showed significant removal, with the highest log removal rate of 3.16-log copies/mL coming for KanR, followed by 2.80-log copies/mL for AmpR and 2.74-log copies/mL for TetA. Overall, the log removal rates of the three ARGs were all greater than 2.74-log copies/mL after 10 min of treatment, though, indicating that lgDBD has high efficiency in removing ARGs.

Fig. 2b-d show the trends in the log degradation rates of AmpR, TetA, and KanR as a function of voltage. These each increased significantly with input voltage. For example, for AmpR, when the input voltage increased from 9 kV to 12 kV, the log removal rate increased from 2.24-log copies/mL to 2.80-log copies/mL. This increase in removal rate is primarily attributable to the enhanced production of ORSs at higher voltages [46–48]. ORSs, such as ·OH and $O_2^{\cdot-}$, are widely recognized as key reactive species in the degradation of resistance genes [49–51]. They react directly with DNA molecules, causing DNA strand breaks or base oxidation, thereby effectively disrupting the structure of ARGs. Different ARGs responded differently to lgDBD treatment due to variations in their molecular and structural characteristics. For instance, AmpR exhibited a significantly higher removal rate than either KanR or TetA. This difference may stem from the relative accessibility of the target sites within the ARGs to ORSs. ARGs with more exposed or flexible structures may be more susceptible to oxidative damage, whereas those with tightly packed or protected structures, may be more resistant to attack [52,53]. Additionally, the chemical composition of ARGs, including the presence of oxidative stress-resistant nucleotide sequences, may also influence their susceptibility to ORSs [54].

Table S2 compares the inactivation efficiency of ARB, the removal efficiency of ARGs, and the electrical energy per order (E_{EO}) across lgDBD, traditional disinfection processes such as UV, chlorine, and ozone, as well as other plasma-based processes. The results show that the lgDBD process achieved > 7.00-log ARB inactivation and 2.74–3.16-log ARGs removal within 10 min, surpassing the performance of most existing plasma-based and conventional disinfection methods. The energy efficiency of lgDBD further highlights its advantages. The E_{EO} of ARB and E_{EO} of ARGs for lgDBD were only 0.268 kWh·m^{-3} and 0.975–1.125 kWh·m^{-3}, respectively, demonstrating a significant advantage over other processes that rely solely on electrical energy consumption. In addition, lgDBD does not require chemical additives, which reduces the risk of secondary pollution and makes it a more environmentally friendly alternative for disinfection technology. Therefore, lgDBD represents a highly competitive solution for AMR control by combining rapid and effective ARB inactivation and ARG removal with exceptional energy efficiency.

3.3. The effects of lgDBD on ARG conjugative transfer

Escherichia coli MG1655 (RP4) was selected as the donor strain for conjugative transfer experimentation, *Escherichia coli* HB101 was used as the intragenus conjugation transfer recipient strain, and *Pseudomonas putida* GDMCC1.445 was used as the intergenus conjugation transfer recipient strain. The minimum inhibitory concentrations of antibiotics for each strain are listed in Table S4. *Escherichia coli* MG1655 has no

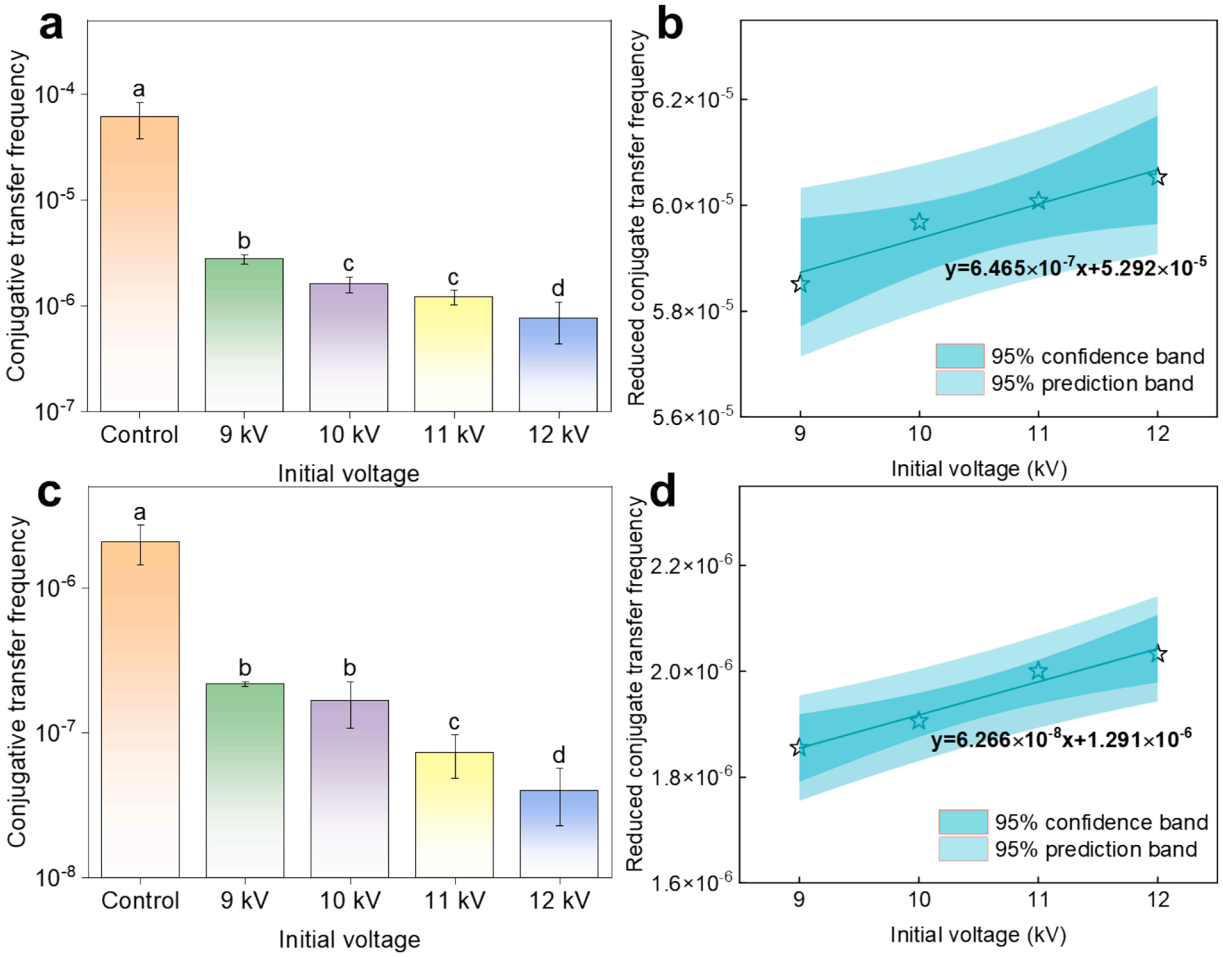

Fig. 3. (a, b) Intragenus conjugation transfer rate and (c, d) intergenus conjugation transfer rate of ARG.

antibiotic resistance, *Escherichia coli* MG1655 (RP4) has Amp and Tet resistance, *Escherichia coli* HB101 has Str resistance, and *Pseudomonas putida* GDMCC1.445 has Chl resistance. In the conjugative transfer experiment, the working concentrations were set as Tet 10 mg/L, Amp 200 mg/L, Str 30 mg/L, and Chl 20 mg/L in order to ensure that different resistance genes were expressed under corresponding conditions and could be effectively monitored.

Fig. 3a shows that prior to lgDBD treatment, the intragenus conjugative transfer frequency of plasmid RP4 from donor *Escherichia coli* MG1655 (RP4) to recipient *Escherichia coli* HB101 was 6.130×10^{-5}. After 10 min of lgDBD treatment at an input voltage of 12 kV, however, the intragenus conjugative transfer frequency significantly decreased to 7.658×10^{-7}, a reduction of 98.6 %. There was no significant difference in the intragenus conjugative transfer frequency under 10 kV and 11 kV. Fig. 3b further illustrates that the reduction in intragenus conjugative transfer frequency correlated positively with input voltage.

Additionally, an intergenus conjugation transfer experiment was conducted between donor *Escherichia coli* MG1655 (RP4) and recipient *Pseudomonas putida* GDMCC1.445 as shown in Fig. 3c-d. Here, prior to lgDBD treatment, the intergenus conjugation transfer rate of plasmid RP4 was 2.073×10^{-6}, significantly lower than the intragenus conjugative transfer frequency. This difference may reflect the natural barrier of intergenus conjugation transfer compared to intragenus conjugation transfer [37]. After 10 min of lgDBD treatment, the intragenus conjugative transfer frequency significantly decreased, with rates of 9 kV (2.175×10^{-7}), 10 kV (1.668×10^{-7}), 11 kV (7.271×10^{-8}), and 12 kV (4.001×10^{-8}), and reductions ranging from 89.5 % to 98.1 %. Overall, lgDBD treatment significantly inhibited both intragenus and intergenus conjugative transfer rate of ARGs, with more pronounced inhibition under high voltage conditions.

The significant inhibition of conjugative transfer rates by lgDBD can be attributed to multiple synergistic mechanisms. First, ORSs generated by lgDBD oxidize and damage key biological macromolecules, including plasmid RP4, that serve as carriers for ARGs. This oxidative damage disrupts the structural integrity and functionality of the plasmids, effectively blocking the transmission pathway of ARGs. Second, the strong electric field in lgDBD induces electroporation, a process that disrupts bacterial cell membranes. Electroporation not only facilitates

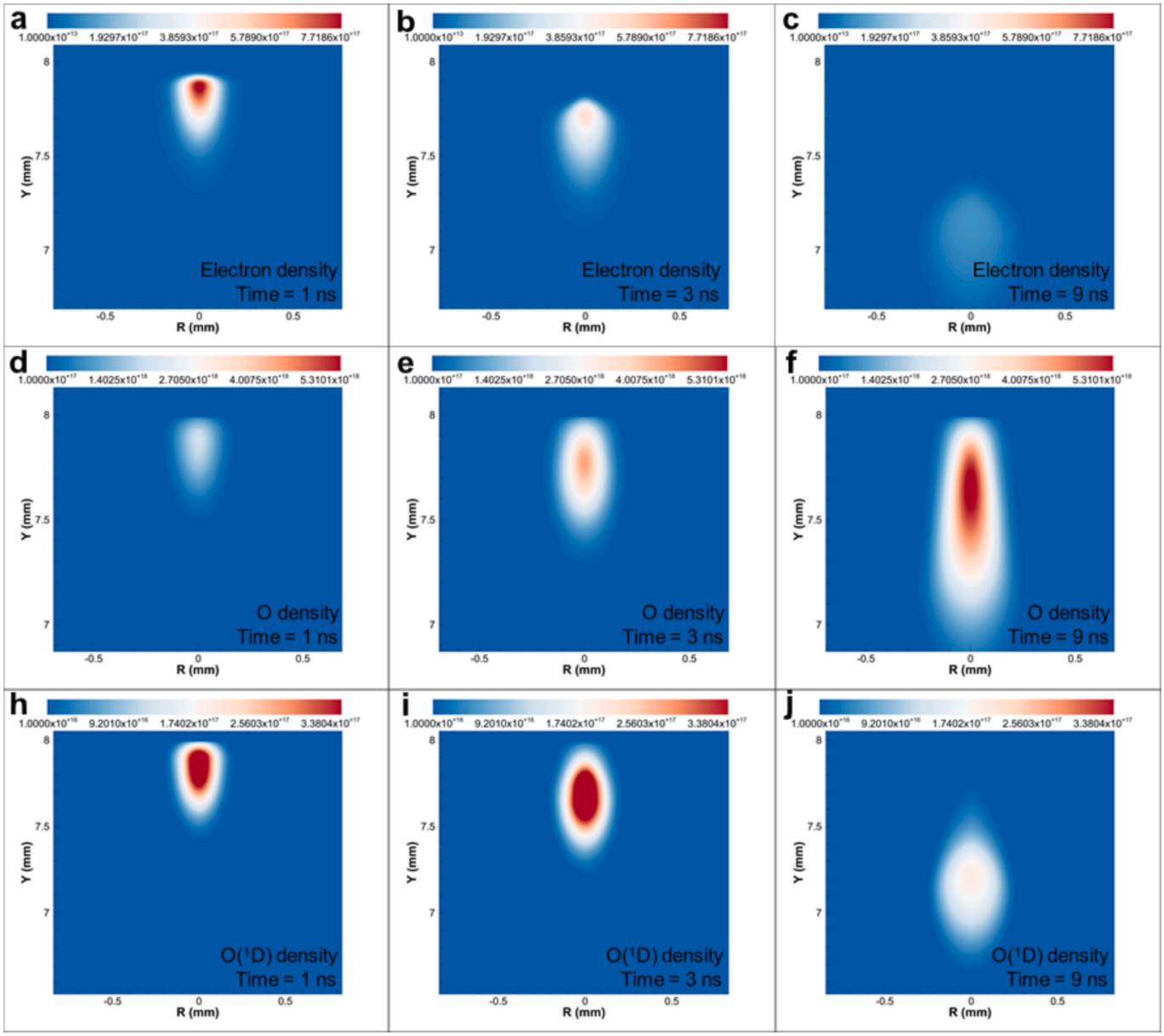

Fig. 4. The basic discharge unit model using PASSKEy code. (a-c) Electron density, (d-f) oxygen density, and (h-j) O(^{1}D) density.

the entry of ORSs into cells, but also causes irreversible damage to bacterial cells, leading to a significant reduction in the number of viable bacteria, which further suppresses conjugative transfer rates [30]. By leveraging this dual mechanism to disrupt the conjugative transfer process between bacteria, lgDBD effectively reduces the risk of ARG dissemination.

3.4. A basic discharge unit model of lgDBD

To understand better the generation and behavior of reactive species during lgDBD discharge, this study constructed a finite element model of the basic discharge unit of lgDBD based using PASSKEy code. Non-thermal plasma is a quasi-neutral medium composed of equal amounts of free electrons and positive ions [55]. Free electrons not only constitute the physical essence of non-thermal plasma but also serve as the main source of its high reactivity [56,57]. Therefore, the density distributions of free electrons and their spatiotemporal variations are crucial for understanding plasma reaction processes. As shown in Fig. 4a-c and Fig. S2, at the onset of discharge, the electron avalanche effect rapidly generates a large number of free electrons (Reactions (1) and (2). This effect occurs as free electrons accelerate under the applied electric field and collide with neutral molecules, releasing more electrons and forming a chain reaction [58]. As the plasma stream propagates, the concentration of free electrons gradually decreases, displaying a non-uniform distribution of free electron density in both space and time, which reflects the plasma propagation conditions.

$$e^- + N_2 = 2e^- + N_2^+ \quad (1)$$

$$e^- + O_2 = 2e^- + O_2^+ \quad (2)$$

In lgDBD, the spatiotemporal distribution of reactive species is the core factor that determines reaction efficiency. Simulation results indicate that the main reactive species generated during lgDBD discharge include free oxygen atoms (O) and excited-state oxygen species ($O(^1D)$) [59]. Free oxygen atoms are produced by collisions between free electrons and oxygen molecules or positive ions (Reactions (3)–(8) and are uniformly generated along the propagation path of the plasma stream (Fig. 4d-f and Fig. S3). These free oxygen atoms can react with molecules at the gas–liquid interface to produce liquid-phase ORSs, which enhance the oxidative capacity of lgDBD. Furthermore, a portion of the free oxygen atoms dissolve directly into water, further promoting the degradation of pollutants in water [60].

$$e^- + O_2 = e^- + O + O \quad (3)$$

$$e^- + O_2 = O^- + O \quad (4)$$

$$e^- + O_4^+ = O + O + O_2 \quad (5)$$

$$e^- + O_2^+ = O + O \quad (6)$$

$$O^- + N_2^+ = O + N + N \quad (7)$$

$$O_2^- + O = e^- + O_2 + O \quad (8)$$

As an excited-state oxygen species, $O(^1D)$ is also abundantly generated during the discharge process, and it plays an important role in the chemical reactions of lgDBD [61]. $O(^1D)$ is primarily formed by collisions between free electrons and O_2 (Reaction (9). Its spatiotemporal distribution is shown in Fig. 4h-j and Fig. S4. Unlike free oxygen atoms, $O(^1D)$ is more concentrated in the tip region of the plasma stream, and this distribution difference is mainly due to the relatively short lifespan of $O(^1D)$, which rapidly diminishes through reactions with O_2 and N_2 where it is converted into free oxygen atoms (Reactions (10)–(11).

$$e^- + O_2 = e^- + O + O(^1D) \quad (9)$$

$$O(^1D) + O_2 = O + O_2 \quad (10)$$

$$O(^1D) + N_2 = O + N_2 \quad (11)$$

The distribution of the electric field intensity during discharge is also noteworthy. As shown in Fig. S5, the electric field intensity within the discharge region varies with the propagation of the plasma streamers, with a maximum value of 2.66×10^6 V/m. Such a high electric field can induce electroporation in bacteria[41], where the strong electric field temporarily disrupts bacterial cell membranes, creating pores that allow the entry of reactive species into the cells. Furthermore, these pores can become permanent under prolonged exposure to high-intensity fields, leading to irreversible membrane damage and cell death. This electroporation effect thus facilitates the interaction between ORSs and biological macromolecules such as plasmids, accelerating the inactivation of ARB and the removal of ARGs.

3.5. The mechanism of ARB and ARG removal by lgDBD

During lgDBD discharge, a large number of oxygen- and nitrogen-based reactive species are generated, and their complex chemical reaction mechanisms pose challenges to deciphering their role in ARB and ARG removal [62,63]. To identify the specific reactive species in lgDBD and their mechanisms of action, we employed EPR analysis in this study. As shown in Fig. 5a, when 5,5-Dimethyl-1-pyrroline N-oxide (DMPO) was used as the spin trap, a clear ·OH peak was detected, indicating the generation of hydroxyl radicals during lgDBD discharge. This generation of ·OH is primarily due to the reaction between $O(^1D)$ and water molecules (Reaction (12). Additionally, some smaller, regular peaks were observed beside the ·OH peak (highlighted in the purple box in Fig. 5a), but due to the low signal intensity, they could not be accurately identified. Based on related literature, these accompanying peaks may be from DMPOO, or they could be overlay of signals from multiple reactive species [28,30]. These observations suggest that the generation of reactive species in lgDBD is complex, requiring further in situ EPR studies for more detailed investigation. As shown in Fig. 5b, when 2,2,6,6-tetramethylpiperidine (TEMP) was used as the spin trap, a 1:1:1 peak appeared, indicating the generation of singlet oxygen ($^1O_2$) during lgDBD. After introducing *Escherichia coli* MG1655 (RP4) bacterial solution, the EPR spectra for ·OH and $^1O_2$ disappeared, however, suggesting that these species had fully reacted with the bacteria and facilitated ARB inactivation. Moreover, the presence of reactive species generated by lgDBD was confirmed through OES (Fig. 5c), which showed the existence of nitrogen excited species and free oxygen atoms, further validating the composition of reactive species produced during lgDBD discharge [64,65].

$$O(^1D) + H_2O \rightarrow H_2O_2^* \rightarrow 2{\cdot}OH \quad (12)$$

To confirm the role of reactive species in the inhibition of conjugative transfer rates in lgDBD, a quenching experiment was also conducted. Tert-butanol (TBA), TEMP, and benzoquinone (BQ) were used as quenchers for ·OH, $^1O_2$, and $O_2^{\cdot-}$, respectively [31], and the results are shown in Fig. 5d. Compared to direct lgDBD treatment, the addition of TBA, TEMP, and BQ resulted in varying degrees of increase in both intragenera and intergenera conjugative transfer rates, which suggests that ·OH, $^1O_2$, and $O_2^{\cdot-}$ all contributed to the inhibition of conjugative transfer rates. The largest increase in conjugative transfer rates was observed with the addition of TBA, indicating that ·OH is the primary reactive species in lgDBD. The addition of TEMP and BQ had a limited inhibitory effect on the intragenera and intergenera conjugative transfer rates, indicating that $^1O_2$ and $O_2^{\cdot-}$ played a secondary role in this process. In summary, ·OH, $^1O_2$, and $O_2^{\cdot-}$ jointly promoted the inhibition of conjugative transfer rates in lgDBD.

In addition, electron microscopy analysis was performed to elucidate the mechanism of ARB inactivation. Fig. S6 shows scanning electron microscope images of ARB before and after lgDBD treatment. The obvious deformation, damage, and lysis of bacteria in Fig. S6b indicate that cell membrane damage was a key factor in ARB inactivation [66,67]. Fig. S7 presents the results of laser confocal microscopy. After

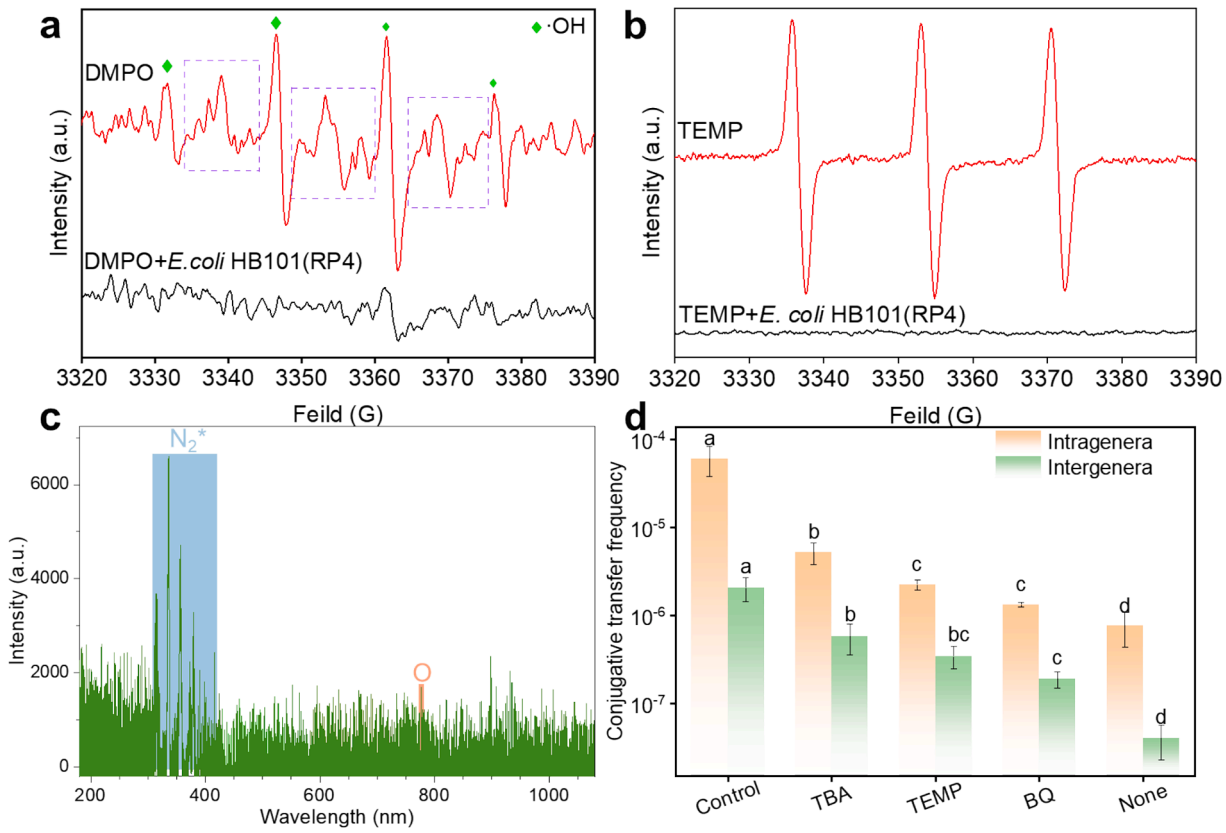

Fig. 5. EPR spectra of (a) DMPO and (b) TEMP; (c) optical emission spectra during plasma discharge; (d) the effect of active substance quencher on intragenera transfer rate and intergenera conjugate transfer rate.

dual staining, live bacteria appeared green, while bacteria with damaged cell membranes appeared red [68]. Hence, after lgDBD treatment, the bacteria transitioned from green to red and yellow, providing visual evidence of cell membrane damage.

Fig. 6 shows a proposed mechanism diagram for lgDBD. During lgDBD treatment, free oxygen atoms and $O(^1D)$ play a key role in the generation and action of reactive species, formed through collisions between free electrons and O_2. $O(^1D)$ reacts with H_2O to generate excited H_2O_2, which rapidly converts into ·OH, and free oxygen atoms collide with O_2 to form O_3. In the water being treated, these reactive species disrupt the integrity of bacterial cell membranes through oxidation and electroporation, inactivating ARB. Furthermore, the reactive species also damage important biological macromolecules such as plasmid RP4, further blocking the spread of ARGs.

The scalability and feasibility of lgDBD for practical water treatment applications both require careful consideration. Although lgDBD has shown promising efficiency in laboratory-scale experiments, several challenges must be addressed for large-scale implementation. One major limitation is the energy consumption associated with maintaining a stable discharge, especially at higher voltages. Further research is needed to optimize the discharge parameters in order to reduce energy consumption without compromising treatment efficiency. Additionally, scaling up the lgDBD system must ensure uniform plasma generation and consistent reactive species distribution across large volumes of water. This may involve designing advanced reactor geometries. In conclusion, lgDBD shows significant potential for controlling ARB and ARGs in water treatment, and future efforts should focus on improving energy efficiency, scaling up system design, and addressing environmental considerations with the goal of ensuring its practical applicability and sustainability.

4. Conclusion

In this study, lgDBD process was applied to inactivate ARB and remove ARGs in water. Experiments demonstrated that under an input voltage of 12 kV, *Escherichia coli* MG1655 (RP4) achieved complete inactivation (>7.00-log) within 8 min. lgDBD exhibited significant removal efficiency for ARGs (AmpR, TetA, and KanR), with log reduction rates exceeding 2.74-log copies/mL after 10 min of treatment. Additionally, lgDBD significantly inhibited the conjugative transfer of ARGs, reducing both intra-species and interspecies transfer rates by more than 98 %, thus minimizing the risk of resistance gene transmission. Furthermore, we clarified the spatiotemporal distribution of key reactive species (such as O and $O(^1D)$) and electric field intensity in the gas-phase plasma by constructing a finite element model. These reactive species generate ORSs at the gas–liquid interface, causing oxidative damage to plasmids and blocking the transmission of ARGs, with the electroporation induced by the strong electric field further facilitating this process. Overall, this study highlights the tremendous potential of the lgDBD process for controlling ARG dissemination and offers new insights into ARG pollution control in water treatment.

CRediT authorship contribution statement

Ruoyu Deng: Writing – review & editing, Writing – original draft, Visualization, Methodology, Formal analysis, Data curation, Conceptualization. **Qiang He:** Writing – review & editing, Project administration, Funding acquisition. **Liang Luo:** Writing – review & editing. **Dongxu Yang:** Writing – review & editing, Validation. **Yi Sun:** Writing – review & editing. **Yi Chen:** Writing – review & editing.

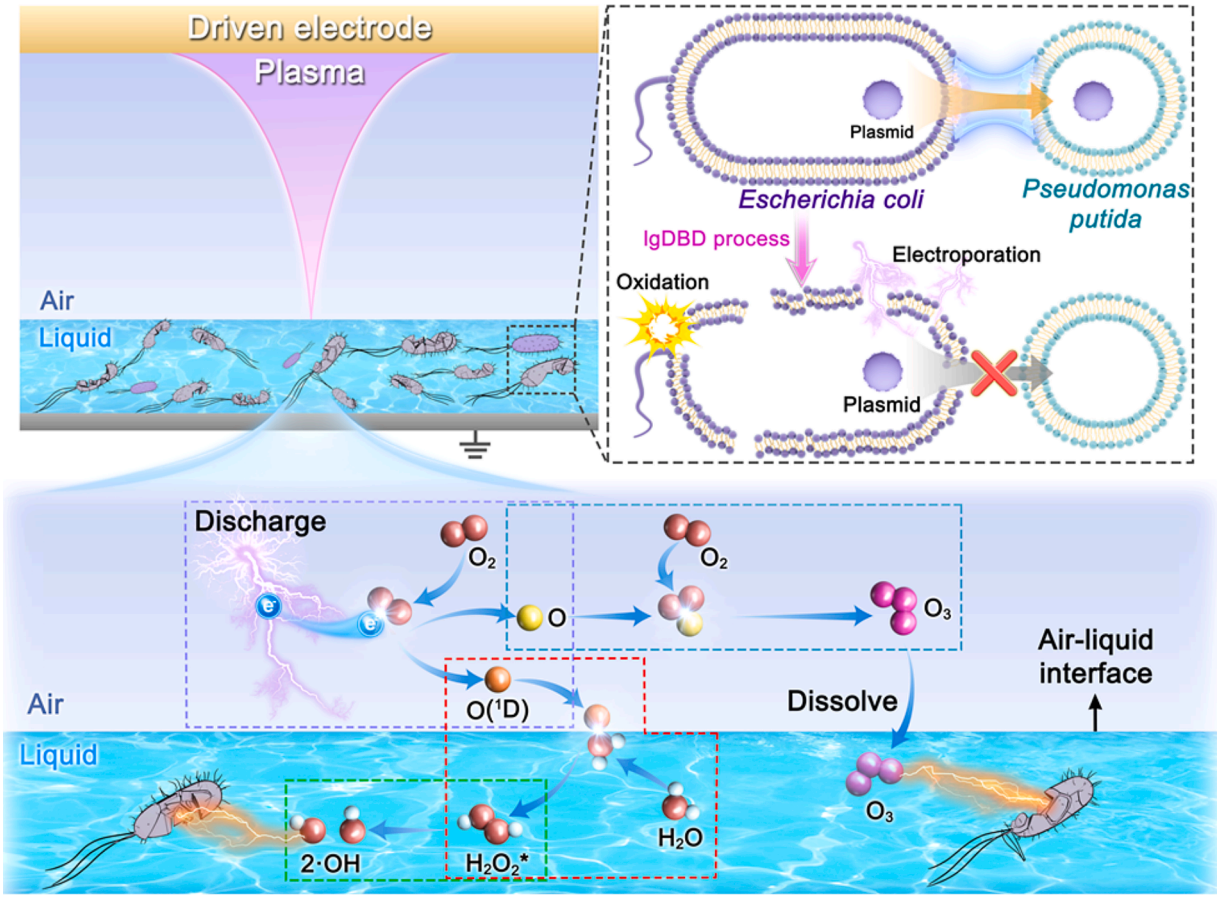

Fig. 6. Inhibition mechanism of antimicrobial resistance in lgDBD.

Declaration of competing interest

The authors declare that they have no known competing financial interests or personal relationships that could have appeared to influence the work reported in this paper.

Acknowledgments

This research was supported by the Chongqing Science Fund for Distinguished Young Scholars (CSTB2022NSCQ-JQX0023). The authors thank AiMi Academic Services (www.aimieditor.com) for English language editing and review services.

Appendix A. Supplementary data

Supplementary data to this article can be found online at https://doi.org/10.1016/j.cej.2025.160485.

Data availability

Data will be made available on request.

References

[1] G. Brandis, J. Larsson, J. Elf Antibiotic perseverance increases the risk of resistance development, Proceedings of the National Academy of Sciences, 120 (2023) e2216216120. doi": 10.1073/pnas.2216216120.
[2] H. Liao, C. Liu, S. Zhou, C. Liu, D.J. Eldridge, C. Ai, S.W. Wilhelm, B.K. Singh, X. Liang, M. Radosevich, Q.-E. Yang, X. Tang, Z. Wei, V.-P. Friman, M. Gillings, M. Delgado-Baquerizo, Y.-G. Zhu, Prophage-encoded antibiotic resistance genes are enriched in human-impacted environments, Nature, Communications 15 (2024) 8315, https://doi.org/10.1038/s41467-024-52450-y.
[3] M.J. Mitcheltree, A. Pisipati, E.A. Syroegin, K.J. Silvestre, D. Klepacki, J.D. Mason, D.W. Terwilliger, G. Testolin, A.R. Pote, K.J.Y. Wu, R.P. Ladley, K. Chatman, A. S. Mankin, Y.S. Polikanov, A.G. Myers, A synthetic antibiotic class overcoming bacterial multidrug resistance, Nature 599 (2021) 507–512, https://doi.org/10.1038/s41586-021-04045-6.
[4] A.N.T. Nguyen, L.C. Woods, R. Gorrell, S. Ramanan, T. Kwok, M.J. McDonald, Recombination resolves the cost of horizontal gene transfer in experimental populations of Helicobacter pylori, Proceedings of the National Academy of Sciences, 119 (2022) e2119010119. doi": 10.1073/pnas.2119010119.
[5] C.L. Brown, A. Maile-Moskowitz, A.J. Lopatkin, K. Xia, L.K. Logan, B.C. Davis, L. Zhang, P.J. Vikesland, A. Pruden, Selection and horizontal gene transfer underlie microdiversity-level heterogeneity in resistance gene fate during wastewater treatment, Nature, Communications 15 (2024) 5412, https://doi.org/10.1038/s41467-024-49742-8.
[6] Q. Zhang, D. Zheng, B. Bai, Z. Ma, S. Zong, Insight into antibiotic removal by advanced oxidation processes (AOPs): Performance, mechanism, degradation pathways, and ecotoxicity assessment, Chem. Eng. J. 500 (2024) 157134, https://doi.org/10.1016/j.cej.2024.157134.
[7] X.-Y. Fan, S.-L. Xu, X. Li, Z.-W. Zhou, Y.-X. Gao, J.-R. Zhao, Z.-X. Zhang, Efficient removal of size-fractionated antibiotic resistance genes (ARGs) in WWTPs secondary effluent by vacuum ultraviolet (VUV) activated potassium peroxymonosulfate (PMS), Chem. Eng. J. 487 (2024) 150779, https://doi.org/10.1016/j.cej.2024.150779.
[8] G. Scarascia, L. Fortunato, Y. Myshkevych, H. Cheng, T. Leiknes, P.-Y. Hong, UV and bacteriophages as a chemical-free approach for cleaning membranes from anaerobic bioreactors, Proceedings of the National Academy of Sciences, 118 (2021) e2016529118. doi": 10.1073/pnas.2016529118.
[9] X. Zhou, Z. Guo, X. Tang, W. Wang, M. Wu, B. Song, Y. Xiang, Y. Li, W. Xiong, D. Huang, C. Zhou, Sulfate radical-based advanced oxidation processes for simultaneous removal of antibiotic-resistant bacteria and antibiotic resistance genes and the affecting factors, Chem. Eng. J. 498 (2024) 155149, https://doi.org/10.1016/j.cej.2024.155149.
[10] S.H. Brodfuehrer, D.C. Blomdahl, D.G. Wahman, G.E. Speitel, P.K. Misztal, L. E. Katz, Simultaneous time-resolved inorganic haloamine measurements enable analysis of disinfectant degradation kinetics and by-product formation, Nature, Water 2 (2024) 434–442, https://doi.org/10.1038/s44221-024-00227-4.
[11] M. Sarkhoshkalat, M.A. Nasab, M.R. Yari, S.S. Tabatabaee, V. Ghavami, F. Joulaei, M. Sarkhosh, Assessment of UV radiation effects on airborne mucormycetes and bacterial populations in a hospital environment, Sci. Rep. 14 (2024) 2708, https://doi.org/10.1038/s41598-024-53100-5.

[12] Q. Yuan, P. Yu, Y. Cheng, P. Zuo, Y. Xu, Y. Cui, Y. Luo, P.J.J. Alvarez, Chlorination (but Not UV Disinfection) Generates Cell Debris that Increases Extracellular Antibiotic Resistance Gene Transfer via Proximal Adsorption to Recipients and Upregulated Transformation Genes, Environ. Sci. Tech. 56 (2022) 17166–17176, https://doi.org/10.1021/acs.est.2c06158.

[13] M. Li, P. Wang, K. Zhang, H. Zhang, Y. Bao, Y. Li, S. Zhan, J.C. Crittenden, Single cobalt atoms anchored on $Ti_3C_2T_x$ with dual reaction sites for efficient adsorption–degradation of antibiotic resistance genes, Proc. Natl. Acad. Sci. 120 (2023) e2305705120, https://doi.org/10.1073/pnas.2305705120.

[14] S. Hogard, R. Pearce, R. Gonzalez, K. Yetka, C. Bott, Optimizing Ozone Disinfection in Water Reuse: Controlling Bromate Formation and Enhancing Trace Organic Contaminant Oxidation, Environ. Sci. Tech. 57 (2023) 18499–18508, https://doi.org/10.1021/acs.est.3c00802.

[15] Z. Li, Y. Hou, Y. Shen, C. Nie, X. Zhang, F. Liu, M. Tong, Oxygen vacancy-dependent synergistic disinfection of antibiotic-resistant bacteria by BiOBr nanoflower induced H_2O_2 activation, Water Res. 267 (2024) 122524, https://doi.org/10.1016/j.watres.2024.122524.

[16] G. Yang, T. Jiang, J. Wen, T. Yu, C. Li, L. Zhang, Reverse water-gas shift in a novel spark-coupled dielectric barrier discharge plasma: Effects of electrode structure and gas parameters, Chem. Eng. J. 499 (2024) 156098, https://doi.org/10.1016/j.cej.2024.156098.

[17] R. De Meyer, Y. Gorbanev, R.-G. Ciocarlan, P. Cool, S. Bals, A. Bogaerts, Importance of plasma discharge characteristics in plasma catalysis: Dry reforming of methane vs. ammonia synthesis, Chem. Eng. J. 488 (2024) 150838, https://doi.org/10.1016/j.cej.2024.150838.

[18] A. Zhang, Y. Zhou, Y. Li, Y. Liu, X. Li, G. Xue, A.C. Miruka, M. Zheng, Y. Liu, Motivation of reactive oxygen and nitrogen species by a novel non-thermal plasma coupled with calcium peroxide system for synergistic removal of sulfamethoxazole in waste activated sludge, Water Res. 212 (2022) 118128, https://doi.org/10.1016/j.watres.2022.118128.

[19] F. Hanon, E.M. Gaigneaux, Post-discharge, An interesting step to improve heterogeneous catalysts synthesized by glidarc plasma? Chem. Eng. J. 489 (2024) 151088 https://doi.org/10.1016/j.cej.2024.151088.

[20] C. Chen, C. Ma, Y. Yang, X. Yang, K. Demeestere, A. Nikiforov, S., Van Hulle, Degradation of micropollutants in secondary wastewater effluent using nonthermal plasma-based AOPs: The roles of free radicals and molecular oxidants, Water Res. 235 (2023) 119881, https://doi.org/10.1016/j.watres.2023.119881.

[21] P. Pareek, S. Kooshki, P. Tóth, M. Janda, Tuning composition of plasma activated water generated by transient spark discharge with electrospray, Chem. Eng. J. 493 (2024) 152583, https://doi.org/10.1016/j.cej.2024.152583.

[22] J. Li, C. Lan, L. Nie, D. Liu, X. Lu, Distributed plasma-water-based nitrogen fixation system based on cascade discharge: Generation, regulation, and application, Chem. Eng. J. 478 (2023) 147483, https://doi.org/10.1016/j.cej.2023.147483.

[23] F. Judée, S. Simon, C. Bailly, T. Dufour, Plasma-activation of tap water using DBD for agronomy applications: Identification and quantification of long lifetime chemical species and production/consumption mechanisms, Water Res. 133 (2018) 47–59, https://doi.org/10.1016/j.watres.2017.12.035.

[24] Y. Su, Y. Yang, W. Jiang, J. Han, H. Guo, A novel strategy of peracetic acid activation by dielectric barrier discharge plasma for bisphenol a degradation: Feasibility, mechanism and active species dominant to degradation pathway, Chem. Eng. J. 476 (2023) 146469, https://doi.org/10.1016/j.cej.2023.146469.

[25] D. Lu, X. Mao, R. Wu, B. Liu, Dielectric Barrier Discharge (DBD) enhanced Fenton process for landfill leachate nanofiltration: Organic matter removal and membrane fouling alleviation, Water Res. 266 (2024) 122358, https://doi.org/10.1016/j.watres.2024.122358.

[26] M. Shaban, N. Merkert, A.C.T. van Duin, D. van Duin, A.P. Weber, Advancing DBD Plasma Chemistry: Insights into Reactive Nitrogen Species such as NO_2, N_2O_5, and N_2O Optimization and Species Reactivity through Experiments and MD Simulations, Environ. Sci. Tech. 58 (2024) 16087–16099, https://doi.org/10.1021/acs.est.4c04894.

[27] J. Lou, H. Han, Z. Zhang, C. Feng, J. An, X. Wang, Citric acid modulated strong magnetic CoFe-LDH/$CoFe_2O_4$ coupled dielectric barrier discharge plasma for efficient levofloxacin degradation: Enhanced internal electric field and accelerated electron migration, J. Hazard. Mater. 480 (2024) 136077, https://doi.org/10.1016/j.jhazmat.2024.136077.

[28] H. Zhang, L. Zhu, Y. Zhang, P. Héroux, L. Cai, Y. Liu, Removal of per- and polyfluoroalkyl substances from water by plasma treatment: Insights into structural effects and underlying mechanisms, Water Res. 253 (2024) 121316, https://doi.org/10.1016/j.watres.2024.121316.

[29] J.-B. Ni, C.-J. Ding, J.-S. Zhang, X.-M. Fang, H.-W. Xiao, Insight into the surface discharge cold plasma efficient inactivation of Pseudomonas fluorescens in water based on exogenous reactive oxygen and nitrogen species: Synergistic mechanism and energy benefits, J. Hazard. Mater. 476 (2024) 134984, https://doi.org/10.1016/j.jhazmat.2024.134984.

[30] R. Deng, Q. He, D. Yang, M. Chen, Y. Chen, Dielectric barrier discharge plasma promotes disinfection-residual-bacteria inactivation via electric field and reactive species, Water Res. 254 (2024) 121386, https://doi.org/10.1016/j.watres.2024.121386.

[31] J. Wu, Q. Xiong, J. Liang, Q. He, D. Yang, R. Deng, Y. Chen, Degradation of benzotriazole by DBD plasma and peroxymonosulfate: Mechanism, degradation pathway and potential toxicity, Chem. Eng. J. 384 (2020) 123300, https://doi.org/10.1016/j.cej.2019.123300.

[32] R. Deng, D. Yang, M. Chen, Q. He, Q. He, Y. Chen, The enhancing energy efficiency of sulfadiazine degradation using a DBD-contact plasma treatment process, Chem. Eng. J. 463 (2023) 142491, https://doi.org/10.1016/j.cej.2023.142491.

[33] I. Adamovich, S. Agarwal, E. Ahedo, L.L. Alves, S. Baalrud, N. Babaeva, A. Bogaerts, A. Bourdon, P.J. Bruggeman, C. Canal, E.H. Choi, S. Coulombe, Z. Donkó, D.B. Graves, S. Hamaguchi, D. Hegemann, M. Hori, H.H. Kim, G.M. W. Kroesen, M.J. Kushner, A. Laricchiuta, X. Li, T.E. Magin, S. Mededovic Thagard, V. Miller, A.B. Murphy, G.S. Oehrlein, N. Puac, R.M. Sankaran, S. Samukawa, M. Shiratani, M. Šimek, N. Tarasenko, K. Terashima, E. Thomas Jr, J. Trieschmann, S. Tsikata, M.M. Turner, I.J. van der Walt, M.C.M. van de Sanden, T. von Woedtke, The 2022 Plasma Roadmap: low temperature plasma science and technology, J. Phys. D Appl. Phys. 55 (2022) 373001, https://doi.org/10.1088/1361-6463/ac5e1c.

[34] B. Yin, Y. Zhu, Y. Wu, Modulating sparks in a pulse train for repetitive and energy efficient plasma generation, High Voltage 8 (2023) 1168–1179, https://doi.org/10.1049/hve2.12348.

[35] I. Adamovich, S.D. Baalrud, A. Bogaerts, P.J. Bruggeman, M. Cappelli, V. Colombo, U. Czarnetzki, U. Ebert, J.G. Eden, P. Favia, D.B. Graves, S. Hamaguchi, G. Hieftje, M. Hori, I.D. Kaganovich, U. Kortshagen, M.J. Kushner, N.J. Mason, S. Mazouffre, S.M. Thagard, H.R. Metelmann, A. Mizuno, E. Moreau, A.B. Murphy, B.A. Niemira, G.S. Oehrlein, Z.L. Petrovic, L.C. Pitchford, Y.K. Pu, S. Rauf, O. Sakai, S. Samukawa, S. Starikovskaia, J. Tennyson, K. Terashima, M.M. Turner, M.C. M. van de Sanden, A. Vardelle, The 2017 Plasma Roadmap: Low temperature plasma science and technology, J. Phys. D Appl. Phys. 50 (2017) 323001, https://doi.org/10.1088/1361-6463/aa76f5.

[36] H. Yang, D. He, L. Fan, F. Cheng, Y. Zhou, Y. Lei, Y.-N. Zhang, X. Yang, J. Qu, Evaluating the Impact of $Cl_2^{\bullet-}$ Generation on Antibiotic-Resistance Contamination Removal via UV/Peroxydisulfate, Environ. Sci. Tech. 58 (2024) 5578–5588, https://doi.org/10.1021/acs.est.3c09952.

[37] H. Zhang, J. Song, Z. Zheng, T. Li, N. Shi, Y. Han, L. Zhang, Y. Yu, H. Fang, Fungicide exposure accelerated horizontal transfer of antibiotic resistance genes via plasmid-mediated conjugation, Water Res. 233 (2023) 119789, https://doi.org/10.1016/j.watres.2023.119789.

[38] Y. Yoon, H.J. Chung, D.Y. Wen Di, M.C. Dodd, H.-G. Hur, Y. Lee, Inactivation efficiency of plasmid-encoded antibiotic resistance genes during water treatment with chlorine, UV, and UV/H_2O_2, Water Res. 123 (2017) 783–793, https://doi.org/10.1016/j.watres.2017.06.056.

[39] Y. Cui, H. Zhao, C. Zhang, Zinc oxide nanoparticles enhance plasmid transfer among growth-promoting endophytes in Arabidopsis thaliana, Sci. Total Environ. 913 (2024) 169682, https://doi.org/10.1016/j.scitotenv.2023.169682.

[40] X. Yang, Y. Chen, T. Liu, L. Zhang, H. Wang, M. Chen, Q. He, G. Liu, F. Ju, Plastic particles affect N_2O release via altering core microbial metabolisms in constructed wetlands, Water Res. 255 (2024) 121506, https://doi.org/10.1016/j.watres.2024.121506.

[41] T. Wang, D.K. Brown, X. Xie, Operando Investigation of Locally Enhanced Electric Field Treatment (LEEFT) Harnessing Lightning-Rod Effect for Rapid Bacteria Inactivation, Nano Lett. 22 (2022) 860–867, https://doi.org/10.1021/acs.nanolett.1c02240.

[42] L. Patinglag, L.M. Melling, K.A. Whitehead, D. Sawtell, A. Iles, K.J. Shaw, Non-thermal plasma-based inactivation of bacteria in water using a microfluidic reactor, Water Res. 201 (2021) 117321, https://doi.org/10.1016/j.watres.2021.117321.

[43] X. Kong, J. Ni, Z. Song, Z. Yang, J. Zheng, Z. Xu, L. Qin, H. Li, Z. Geng, J. Zeng, Synthesis of hydroxylamine from air and water via a plasma-electrochemical cascade pathway, Nat. Sustainability 7 (2024) 652–660, https://doi.org/10.1038/s41893-024-01330-w.

[44] H. Xu, Y. Zhu, M. Du, Y. Wang, S. Ju, R. Ma, Z. Jiao, Subcellular mechanism of microbial inactivation during water disinfection by cold atmospheric-pressure plasma, Water Res. 188 (2021) 116513, https://doi.org/10.1016/j.watres.2020.116513.

[45] T. Wang, X. Xie, Nanosecond bacteria inactivation realized by locally enhanced electric field treatment, Nat. Water 1 (2023) 104–112, https://doi.org/10.1038/s44221-022-00003-2.

[46] J. Zhou, T. Wang, X. Xie, Locally Enhanced Electric Field Treatment (LEEFT) Promotes the Performance of Ozonation for Bacteria Inactivation by Disrupting the Cell Membrane, Environ. Sci. Tech. 54 (2020) 14017–14025, https://doi.org/10.1021/acs.est.0c03968.

[47] R. Li, O.F. Isowamwen, K.C. Ross, T.M. Holsen, S.M. Thagard, PFAS–CTAB Complexation and Its Role on the Removal of PFAS from a Lab-Prepared Water and a Reverse Osmosis Reject Water Using a Plasma Reactor, Environ. Sci. Tech. 57 (2023) 12901–12910, https://doi.org/10.1021/acs.est.3c03679.

[48] Y. Xu, N. Liu, Y. Lin, X. Mao, H. Zhong, Z. Chang, M.N. Shneider, Y. Ju, Enhancements of electric field and afterglow of non-equilibrium plasma by Pb(Zr_xTi_{1-x})O_3 ferroelectric electrode, Nat. Commun. 15 (2024) 3092, https://doi.org/10.1038/s41467-024-47230-7.

[49] W. Liu, M. Xia, C. Zhao, B. Chong, J. Chen, H. Li, H. Ou, G. Yang, Efficient ammonia synthesis from the air using tandem non-thermal plasma and electrocatalysis at ambient conditions, Nat. Commun. 15 (2024) 3524, https://doi.org/10.1038/s41467-024-47765-9.

[50] H. Guo, S. Pan, Z. Hu, Y. Wang, W. Jiang, Y. Yang, Y. Wang, J. Han, Y. Wu, T. Wang, Persulfate activated by non-thermal plasma for organic pollutants degradation: A review, Chem. Eng. J. 470 (2023), https://doi.org/10.1016/j.cej.2023.144094.

[51] T. Wang, Y. Cao, G. Qu, Q. Sun, T. Xia, X. Guo, H. Jia, L. Zhu, Novel Cu(II)–EDTA Decomplexation by Discharge Plasma Oxidation and Coupled Cu Removal by Alkaline Precipitation: Underneath Mechanisms, Environ. Sci. Tech. 52 (2018) 7884–7891, https://doi.org/10.1021/acs.est.8b02039.

[52] C. Ye, M. Feng, Y. Chen, Y. Zhang, Q. Chen, X. Yu, Dormancy induced by oxidative damage during disinfection facilitates conjugation of ARGs through enhancing

efflux and oxidative stress: A lagging response, Water Res. 221 (2022) 118798, https://doi.org/10.1016/j.watres.2022.118798.
[53] Z. Liu, L. Feng, B. Li, C. Lü, J. Sun, S. Giannakis, Crouching bacteria, hidden tetA genes in natural waters: Intracellular damage via double persulfate activation (UVA/Fe^{2+}/PDS) effectively alleviates the spread of antibiotic resistance, J. Hazard. Mater. 480 (2024) 135854, https://doi.org/10.1016/j.jhazmat.2024.135854.
[54] J. Cadet, K.J.A. Davies, Oxidative DNA damage & repair: An introduction, Free Radical Biology and Medicine, 107 (2017) 2-12. 10.1016/j.freeradbiomed.2017.03.030.
[55] F.L. Li, C.T. Hung, K.M. Lin, T.C. Wei, J.S. Wu, Numerical and experimental investigation of light emissions of a planar nitrogen atmospheric-pressure dielectric barrier discharge due to addition of ammonia considering oxygen impurity, Plasma Sources Sci. Technol. 22 (2013) 065003, https://doi.org/10.1088/0963-0252/22/6/065003.
[56] X. Mao, H. Zhong, T. Zhang, A. Starikovskiy, Y. Ju, Modeling of the effects of non-equilibrium excitation and electrode geometry on H_2/air ignition in a nanosecond plasma discharge, Combust. Flame 240 (2022) 112046, https://doi.org/10.1016/j.combustflame.2022.112046.
[57] X. Chen, Y. Zhu, Y. Wu, Modeling of streamer-to-spark transitions in the first pulse and the post discharge stage, Plasma Sources Sci. Technol. 29 (2020) 095006, https://doi.org/10.1088/1361-6595/ab8e4e.
[58] W.H. Zhou, D.X. Zhang, X.H. Duan, X. Zhu, F. Liu, Z. Fang, Effect of dielectric material on the uniformity of nanosecond pulsed dielectric barrier discharge, Plasma Sci. Technol 26 (2024) 094008, https://doi.org/10.1088/2058-6272/ad5fe6.
[59] A.V. Volynets, D.V. Lopaev, T.V. Rakhimova, O.V. Proshina, A.A. Chukalovsky, J. P. Booth, Fast quenching of metastable $O_2(a^1\Delta_g)$ and $O_2(b^1\sigma_g^+)$ molecules by $O(^3P)$ atoms at high temperature, Plasma Sources Sci. Technol. 29 (2020) 115020, https://doi.org/10.1088/1361-6595/abbf92.
[60] J.M. Rimsza, J.A. Kelber, J.C. Du, Mechanisms of oxygen plasma damage of amine and methyl terminated organosilicate low-k dielectrics from ab initio molecular dynamics simulations. Journal of Physics D-Applied, Physics 47 (2014) 335204, https://doi.org/10.1088/0022-3727/47/33/335204.
[61] A.V. Volynets, D.V. Lopaev, S.M. Zyryanov, M.A. Bogdanova, A.T. Rakhimov, Volume and surface loss of $O(^3P)$ atoms in O_2 RF discharge in quartz tube at intermediate pressures (10-100 Torr), Journal of Physics D-Applied, Physics 52 (2019) 395203, https://doi.org/10.1088/1361-6463/ab28dc.
[62] Y. Wang, W. Jiang, J. Han, W. Qiao, H. Guo, An in-depth insight into the simultaneous oxidation of sulfamethoxazole and reduction of Cr (VI) by one system of water film DBD plasma: The interaction effect, role of active species, and their dominant to pathways, Chemosphere 333 (2023), https://doi.org/10.1016/j.chemosphere.2023.138958.
[63] T. Shen, H. Yu, P. Wang, X. Wang, C. Yang, P. Xu, J. Qu, G. Zhang, Layered double oxide/copper foam actuates dielectric barrier discharge plasma via electron transport: Exploring the reactive species evolution and diuron disassembly routes, Appl Catal B 336 (2023) 122950, https://doi.org/10.1016/j.apcatb.2023.122950.
[64] Y. Tang, H. Zhang, J. Yan, N. Luo, X. Fu, X. Wu, J. Wu, C. Liu, D. Zhang, Assessing the efficacy of bleaching powder in disinfecting marine water: Insights from the rapid recovery of microbiomes, Water Res. 241 (2023) 120136, https://doi.org/10.1016/j.watres.2023.120136.
[65] R.J.N. Aka, S. Wu, D. Mohotti, M.A. Bashir, A. Nasir, Evaluation of a liquid-phase plasma discharge process for ammonia oxidation in wastewater: Process optimization and kinetic modeling, Water Res. 224 (2022) 119107, https://doi.org/10.1016/j.watres.2022.119107.
[66] L.C. Kennedy, V.P. Costantini, K.A. Huynh, S.K. Loeb, W.C. Jennings, S. Lowry, M. C. Mattioli, J. Vinjé, A.B. Boehm, Persistence of Human Norovirus (GII) in Surface Water: Decay Rate Constants and Inactivation Mechanisms, Environ. Sci. Tech. 57 (2023) 3671–3679, https://doi.org/10.1021/acs.est.2c09637.
[67] J. Wang, W. Chen, T. Wang, E. Reid, C. Krall, J. Kim, T. Zhang, X. Xie, C.-H. Huang, Bacteria and Virus Inactivation: Relative Efficacy and Mechanisms of Peroxyacids and Chlor(am)ine, Environ. Sci. Tech. 47 (2023) 18710–18721, https://doi.org/10.1021/acs.est.2c09824.
[68] J.-X. Xu, G.-Q. Chen, Y.-L. Chen, H.-M. Wu, D. Chen, H. Liu, Nanowire-assisted electroporation via inducing cell destruction for inhibiting formation of VBNC bacteria: Comparison with chlorination, Water Res. 258 (2024) 121776, https://doi.org/10.1016/j.watres.2024.121776.